ELECTRONIC SUPPLEMENTARY INFORMATION

Dioxygen-Halogen Bonding Exemplified by Crystalline Peroxosolvates of N,N'-bis(haloacetyl) Bispidines

Alexander G. Medvedev,[a] Aleksei V. Medved'ko,[b] Mikhail V. Vener,[a] Andrei V. Churakov,[a] Petr V. Prikhodchenko*[a] and Sergey Z. Vatsadze*[b]

[a] Kurnakov Institute of General and Inorganic Chemistry, Russian Academy of Sciences, Moscow 119991, Russian Federation; e-mail: prikhman@gmail.com
[b] N. D. Zelinsky Institute of Organic Chemistry, Russian Academy of Sciences, Moscow 119991, Russian Federation; e-mail: zurabych@gmail.com

Experimental Section.

Materials.

Aqueous 50 wt% hydrogen peroxide was purchased from Sigma-Aldrich. 96 wt% hydrogen peroxide was prepared from serine peroxosolvate.[1] The concentration of hydrogen peroxide was determined by permanganometry.

Safety note. Caution! Concentrating hydrogen peroxide solutions and working with them require safety precautions.[2]

Glassware for peroxide rich solutions: All glassware were treated by filling with 1M NaOH for 1 day, then with 1M nitric acid for an additional day, and finally with 10 wt.% hydrogen peroxide for an further day. Chromosulfuric acid or permanganate treatment should be avoided.

Synthesis.

Bis(haloacetyl)-containing bispidines (Scheme S1) were obtained according with previously reported procedures.[3,4] Briefly, bromine and chlorine containing compounds were obtained by bridge opening in 5,7-dimethyl-1,3-diazadamantanes with the corresponding haloacetyl halides.[4] The corresponding iodo derivatives were prepared from chlorides by the Finkelstein halogen exchange.[5]

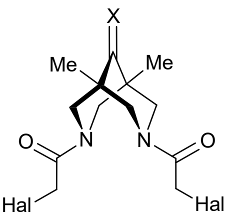

1': Hal=I, X=2H
2': Hal=Br, X=2H
2'': Hal=Cl, X=2H
3': Hal=I, X=O
4': Hal=Br, X=O
5': Hal=Cl, X=O

Scheme S1. The structures of title organic compounds **1'-5'**.

Synthesis of $C_{13}H_{20}I_2N_2O_2{\cdot}H_2O_2$ (1). 20 mg of bispidine $C_{13}H_{20}I_2N_2O_2$ (**1'**, Scheme 1) was dissolved in 0.3 mL of 96% H_2O_2 at 0°C. The colourless crystals were obtained from the mother liquor after cooling at -20°C for 12 h.

Synthesis of $C_{13}H_{20}I_2N_2O_2{\cdot}H_2O_2$ (2). 30 mg of bispidine $C_{13}H_{20}Br_2N_2O_2$ (**2'**) was dissolved in 0.3 mL of 96% H_2O_2 at 0°C. The colourless crystals were obtained from the mother liquor after cooling at -20°C for 12 h.

Synthesis of $C_{13}H_{20}I_2N_2O_5{\cdot}0.5H_2O_2$ (3). 30 mg of bispidine $C_{13}H_{18}I_2N_2O_3$ (**3'**) was dissolved in 0.3 mL of 96% H_2O_2 at 0°C. The colourless crystals were obtained from the mother liquor after cooling at -20°C for 12 h.

Synthesis of $C_{13}H_{20}Br_2N_2O_5{\cdot}H_2O_2$ (4). 30 mg of bispidine $C_{13}H_{18}Br_2N_2O_3$ (**4'**) was dissolved in 0.3 mL of 96% H_2O_2 at 0°C. The colourless crystals were obtained from the mother liquor after cooling at -20°C for 12 h.

*Synthesis of $C_{13}H_{20}Cl_2N_2O_5{\cdot}H_2O_2$ (**5**).* 40 mg of bispidine $C_{13}H_{18}Cl_2N_2O_3$ (**4'**) was dissolved in 0.3 mL of 96% H_2O_2 at 0°C. The colourless crystals were obtained from the mother liquor after cooling at -20°C for 12 h.

Characterization.

SCXRD. Single crystal X-ray diffraction. Single crystals of **2**-**5** suitable for X-ray analysis were collected from the corresponding solutions of **1'**-**5'**, respectively, in 96 wt.% hydrogen peroxide cooled to -20°C without further recrystallization. Experimental intensities were measured on a Bruker D8 Venture diffractometer at 100 K and Bruker SMART APEX II at 100 K (graphite monochromatized MoK_{α} radiation, λ = 0.71073 Å) using ω-scan mode. Absorption corrections based on measurements of equivalent reflections were applied.[6] The structures were solved by direct methods and refined by full matrix least-squares on F^2 with anisotropic thermal parameters for all non-hydrogen atoms.[7] Hydrogen atoms of alkyl fragments in **2**-**5**, minor component of disordered H_2O_2 molecule in **2**, hydroperoxo/hydroxo fragments in **3** were placed in calculated positions and refined using a riding model. Hydrogen atoms of hydrogen peroxide molecules in **2**-**5** and hydroperoxo/hydroxo fragments in **4, 5** were localized objectively, and their positional parameters were refined with restrained O–H distances (DFIX).
X-ray diffraction studies were performed at the Centre of Shared Equipment of IGIC RAS. Selected crystallographic data are provided in Table S9. The crystallographic data for **2**-**5** have been deposited with the Cambridge Crystallographic Data Centre as supplementary publications under the CCDC numbers 2289223-2289226, respectively.

Infrared spectroscopy. Fourier-transform infrared spectroscopy (FTIR) spectra were recorded on a JASCO FT/IR-4600 spectrometer equipped with ATR PRO ONE Single-reflection ATR accessory (Figs. S7-S11).

Differential scanning calorimetry (DSC) measurements were performed on differential scanning calorimeter, DSC-60 Plus (Shimadzu) under argon flow at a heating rate of 5 °C/min (Figs. S2-S6).

Computational details

Hirshfeld Surface Analysis

The Hirshfeld surface analysis[8] of the hydrogen peroxide and organic hydroperoxide and peroxide molecules in **1**-**3**, **6** was performed in the CrystalExplorer program (ver. 21.5)[9] at "high" quality of surface resolution using the corresponding crystallographic information files. The distances from the Hirshfeld surface to the nearest nucleus outside and inside the surface (d_e and d_i, respectively) were plotted into a 2D fingerprint map, and the contributions from the contacts between different atom pairs were evaluated.

Periodic (Solid-State) DFT calculations

Density functional theory computations with periodic boundary conditions (solid-state DFT) were performed by the Crystal17 software package[10] using B3LYP functional in the localized basis set

6-31G** for C, H, N, O atoms and pob-TZVP for I and Br atoms.[11] the use of long-range corrected CAM-B3LYP and dispersion corrected PBE-D3 with Becke–Jones damping function developed by Grimme et al.[12,13] results in imaginary frequencies.

The space groups and unit cell parameters of the considered two-component crystals (**1**-**3**, **6**) obtained in the single-crystal X-ray studies are fixed and structural relaxations are limited to the positional parameters of atoms (ATOMONLY). The atomic positions from experiment are used as the starting point in the solid-state DFT computations. The model structure of **1**, **2** and **6** were obtained from the crystal structure, which has one crystallographically independent hydrogen peroxide molecule disordered over two sites and disordered peroxide group in **6**. Only the higher occupancy was considered in our computations. The B3LYP/6-31G** approximation provides reliable and consistent results in studying the intermolecular interactions in crystals. The mixing coefficient of Hartree-Fock/Kohn-Sham matrices is set to 25%. Tolerance on energy controlling the self-consistent field convergence for geometry optimizations and frequencies computations is set to 10^{-10} and 10^{-11} hartree respectively. The shrinking factor of the reciprocal space net is set to 3. All the optimized structures are found to correspond to the minimum point on the potential energy surface.

Identification of non-covalent interactions through reduced density gradient (RDG)

The optimized structures were used in B3LYP/6-31G** computations of the periodic electronic density. Electron density ρ, Laplacian of the electron density $\nabla^2\rho$ and magnitude of the gradient of electron density $|\nabla\rho|$ three-dimensional grid files were prepared by Topond14.[14] The functions are plotted in a volume corresponding to the conventional unit cell as a set of CUBE format files (3DRHOO, 3DLAPP, 3DGRHO).

The CUBE files were post processed by the NCIMilano public code[15] and the quantities of reduced density gradient (RDG) and ρ*sign(λ_2) (i.e. the electron density multiplied by the sign second greatest eigenvalue of the electron density Hessian matrix) were calculated (RDG and rhosign keywords, respectively). The RDG was calculated in a range of ρ(r) values from -0.05 to 0.05. The RDG isosurfaces have been drawn with the VMD software[16] using the calculated CUBE files.

Evaluation of non-covalent interaction energies

The quantum theory of atoms in molecules and crystals (Bader) analysis of the crystalline electron density[17,18] is performed with TOPOND14.[14] The calculation methodology is presented elsewhere.[19,20] The energy of the considered non-covalent interaction, energy E_{int}, is evaluated according to several procedures. Namely, according to ref. [21] as:

$$E_{int}\ [\text{a.u.}] = -1/2\cdot V_b\ [\text{a.u.}], \qquad \text{(Eq. S1)}$$

refs. [22,23] as:

$$E_{int}\ [\text{a.u.}] = 0.429\cdot G_b\ [\text{a.u.}], \qquad \text{(Eq. S2)}$$

ref. [24] as:

$$E_{int}\ [\text{a.u.}] = -\beta\cdot V_b\ [\text{a.u.}], \qquad \text{(Eq. S3)}$$

and

$$E_{int}\ [\text{a.u.}] = -\gamma\cdot G_b\ [\text{a.u.}], \qquad \text{(Eq. S4)}$$

where V_b and G_b are the local electronic potential and kinetic energy densities, respectively, at the O-H…O and C-Hal…O bond critical point, where Hal=Br, I; the coefficients of proportionality β and γ are equal to 0.58 and 0.57 for bromine atom and 0.68 and 0.67 for iodine atom. Eqs. S1 and S2 was initially developed for hydrogen bonding, while Eqs. S3 and S4 was specifically developed for non-covalent interactions involving halogen atoms. Eqs. S3 and S4 overestimate E_{int} values (Table S8) in comparison with published data.[25]

Gas phase calculations

FTIR spectra of diacetone diperoxide (DADP) and diacetone diperoxide -triodotrinitrobenzene (DADP·TITNB) 1:1 and 1:2 halogen bonded complexes were calculated with Gaussian09 software[26] using B3LYP functional and 6-311++G** basis set for C, H, N, O atoms and Def2-TZVP basis set for I atoms

Crystal structure of peroxosolvates without halogen bonding.

Peroxosolvates of bromo- and chloro-containing hydroperoxo/hydroxo bispidines, $C_{13}H_{20}Br_2N_2O_5 \cdot H_2O_2$ (**4**) and $C_{13}H_{20}Cl_2N_2O_5 \cdot H_2O_2$ (**5**), respectively, are isomorphous and crystallizes in *C*2/*c* space group. The asymmetric unit contains one centrosymmetric organic coformer and hydrogen peroxide (Fig. S1). The O=C–C–Hal fragments of coformer are planar with torsion angle less than 5°. As in **3**, hydroperoxo and hydroxo groups are disordered with 0.5 occupancy ratio. The O(2) oxygen atom is shared between hydroxo and hydroperoxo groups. Both fragments act as a hydrogen donor in H-bond with hydrogen peroxide in **4** and **5** (Fig. S1, Table S4). The H_2O_2 molecule forms four hydrogen bonds, two of them as donors of proton with carbonyl oxygen atom as in **1-3**. The detailed analysis of the crystal data did not reveal the formation of any kind of halogen bonding in **4** and **5**. The conformation of O=C–C–Hal fragments in **4** and **5** does not promote halogen bond formation with hydrogen peroxide molecules in comparison with the structures of **1-3** with O=C–C–Hal torsion angles close to 90°. It should be noted that **4** and **5** are the examples of crystalline hydrogen peroxide adducts of compounds containing organic hydroperoxide fragments (C-OOH) with intermolecular hydrogen bonds between hydroperoxo groups and H_2O_2 molecules.

Supplementary Figures

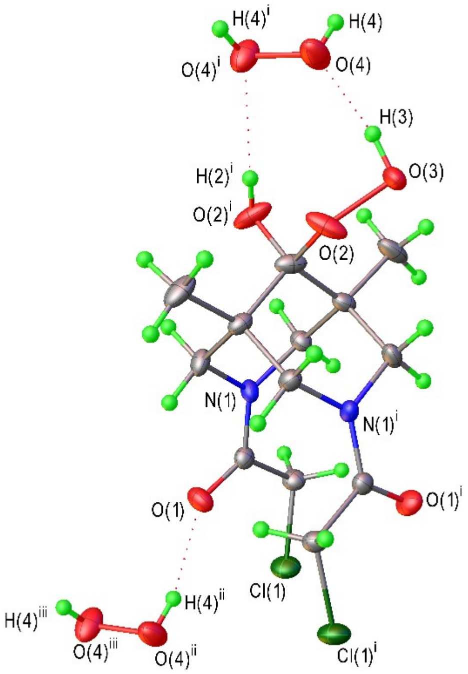

Fig. S1. Molecular structure of **5**. Hydrogen bonds are shown with dashed red lines. Displacement ellipsoids are drawn at 50% probability level. The second components of disordered hydroxo and hydroperoxo fragment is not shown for clarity. i: -X+1, Y, -Z+1/2; ii: X-1/2, Y+1/2, Z; iii: -X+1/2, Y+1/2, -Z+1/2.

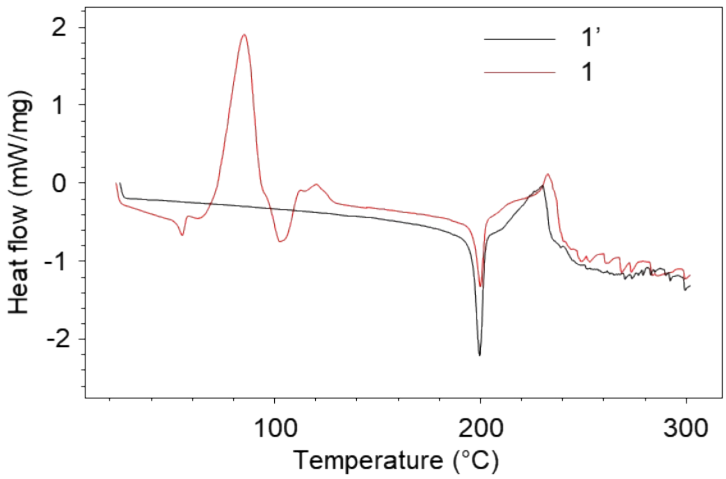

Fig. S2. DSC curves of bispidine **1'** and peroxosolvate **1**.

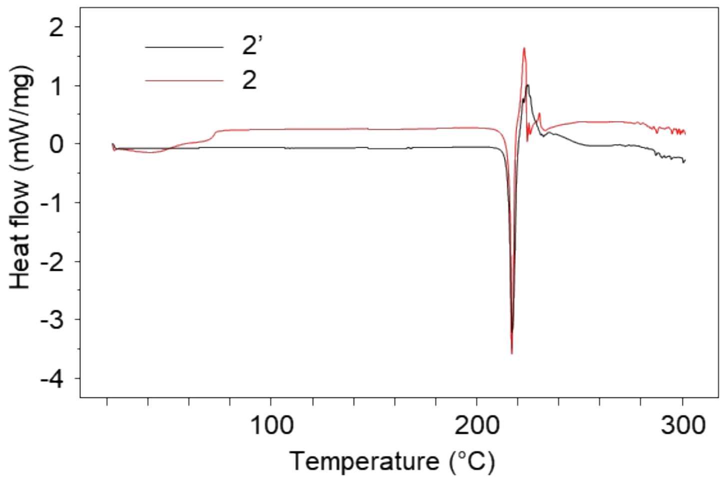

Fig. S3. DSC curves of bispidine **2'** and peroxosolvate **2**.

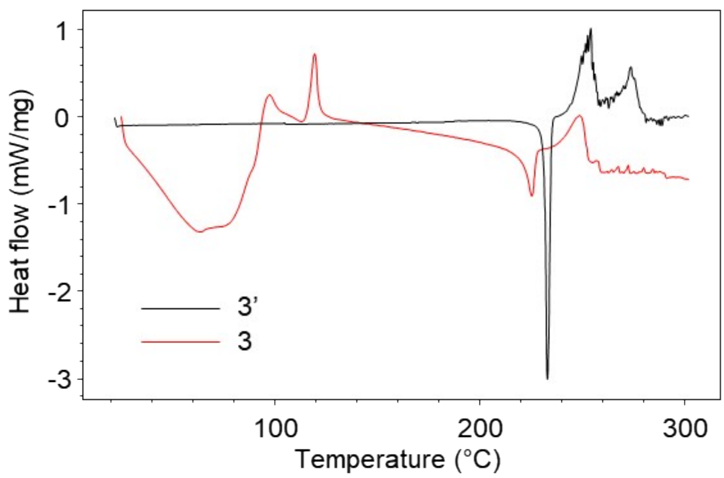

Fig. S4. DSC curves of bispidine **3'** and peroxosolvate **3**.

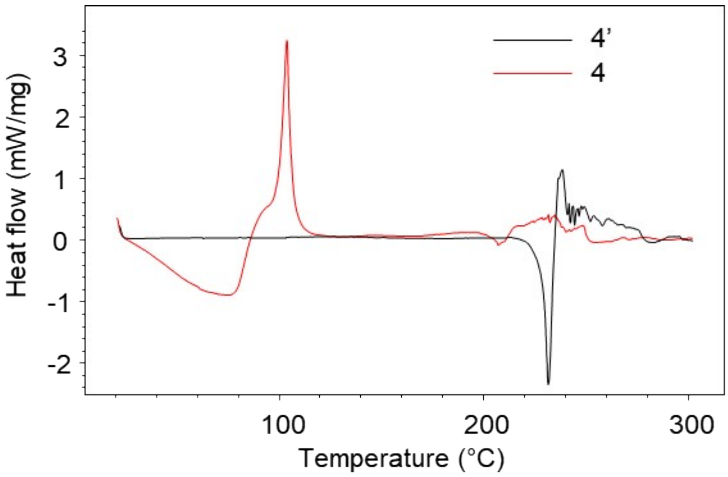

Fig. S5. DSC curves of bispidine **4'** and peroxosolvate **4**.

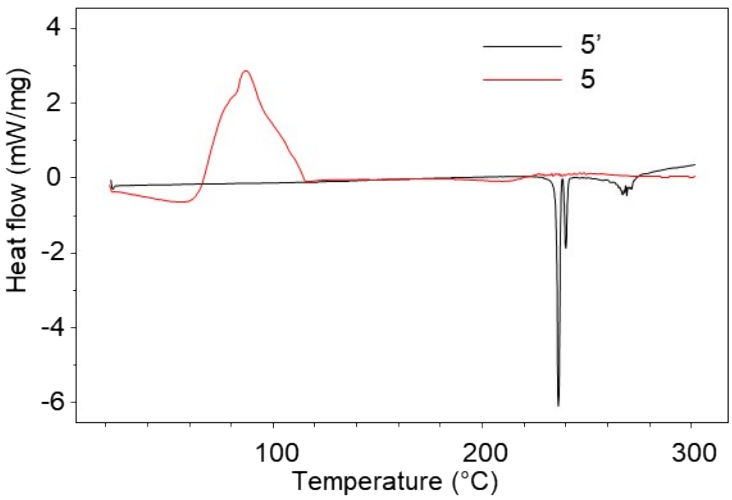

Fig. S6. DSC curves of bispidine **5'** and peroxosolvate **5**.

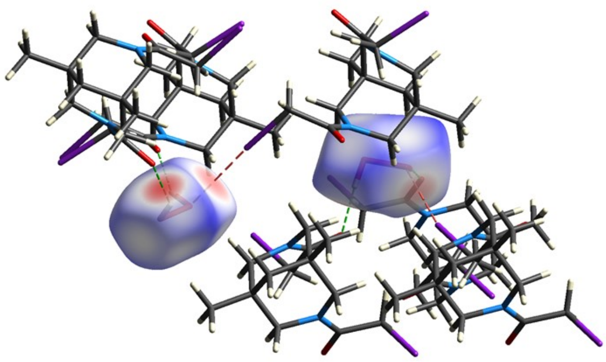

Fig. S7. Hirshfield surfaces of hydrogen peroxide molecule mapped over a d_{norm} range in **1**.

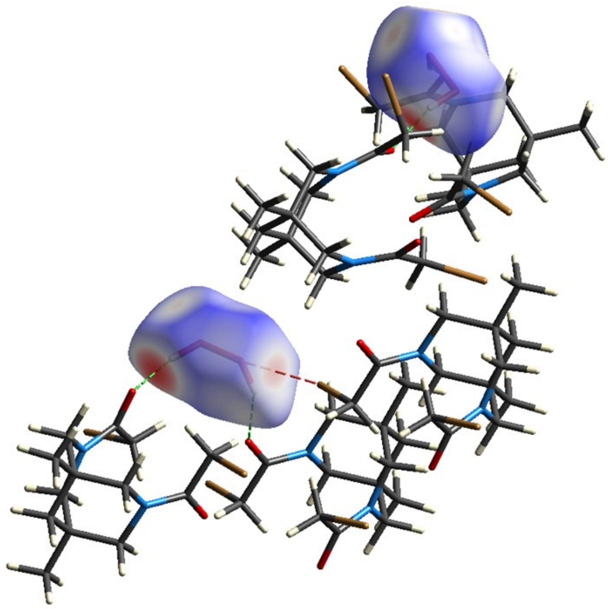

Fig. S8. Hirshfield surfaces of hydrogen peroxide molecule mapped over a d_{norm} range in **2**.

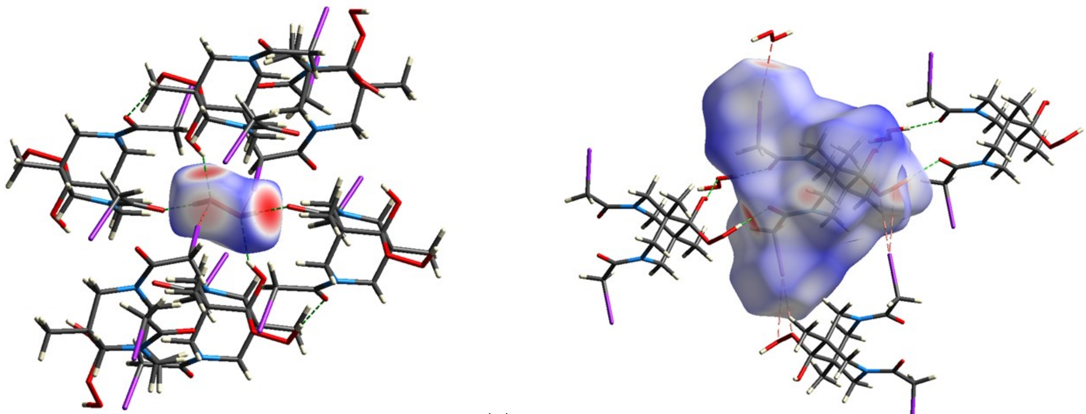

(a) (b)

Fig. S9. Hirshfield surfaces of hydrogen peroxide molecule (a) and organic moiety (b) mapped over a d_{norm} range in 3.

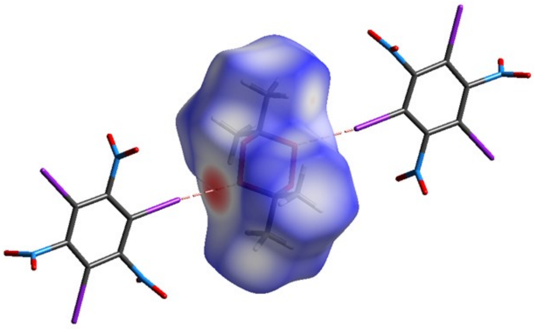

Fig. S10. Hirshfield surfaces of diacetone diperoxide molecule mapped over a d_{norm} range in **2**.

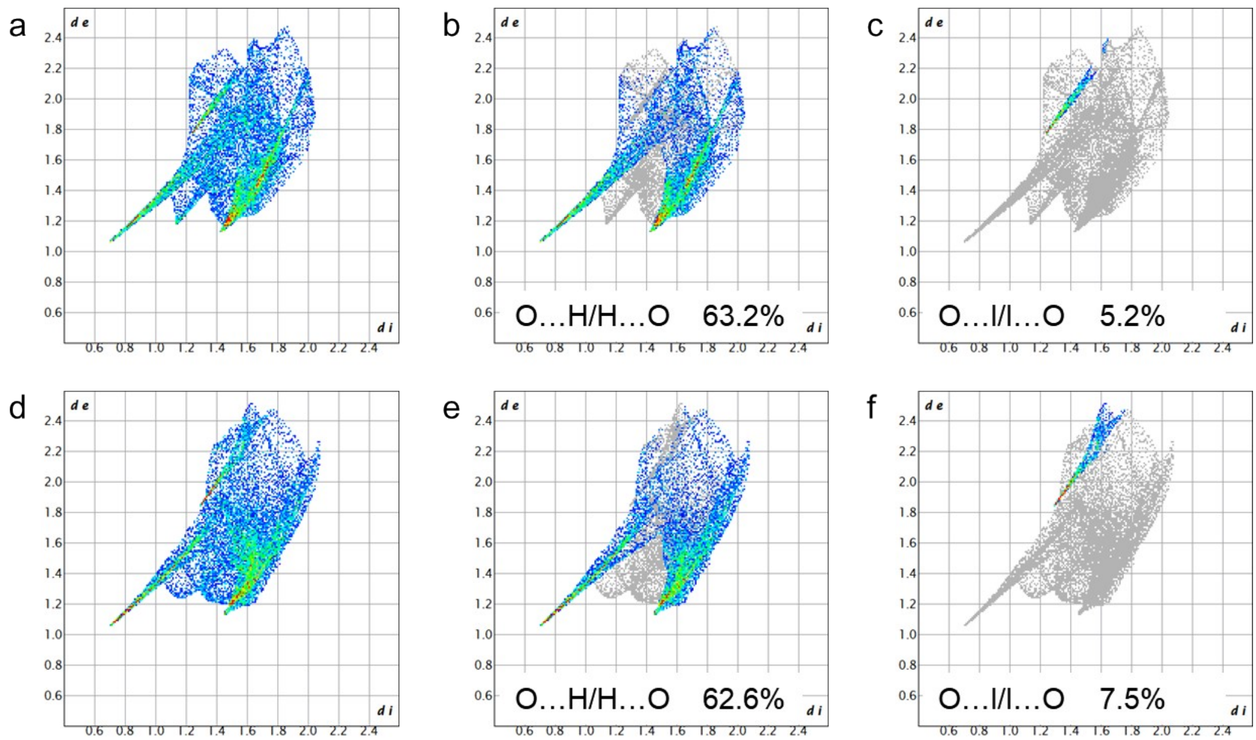

Fig. S11. Fingerprint plots: full (a,d) and resolved into O…H/H…O (b,e) and O…I/I…O (c,f) contacts for two crystallographically independent hydrogen peroxide molecules (top and down rows, respectively) in **1**.

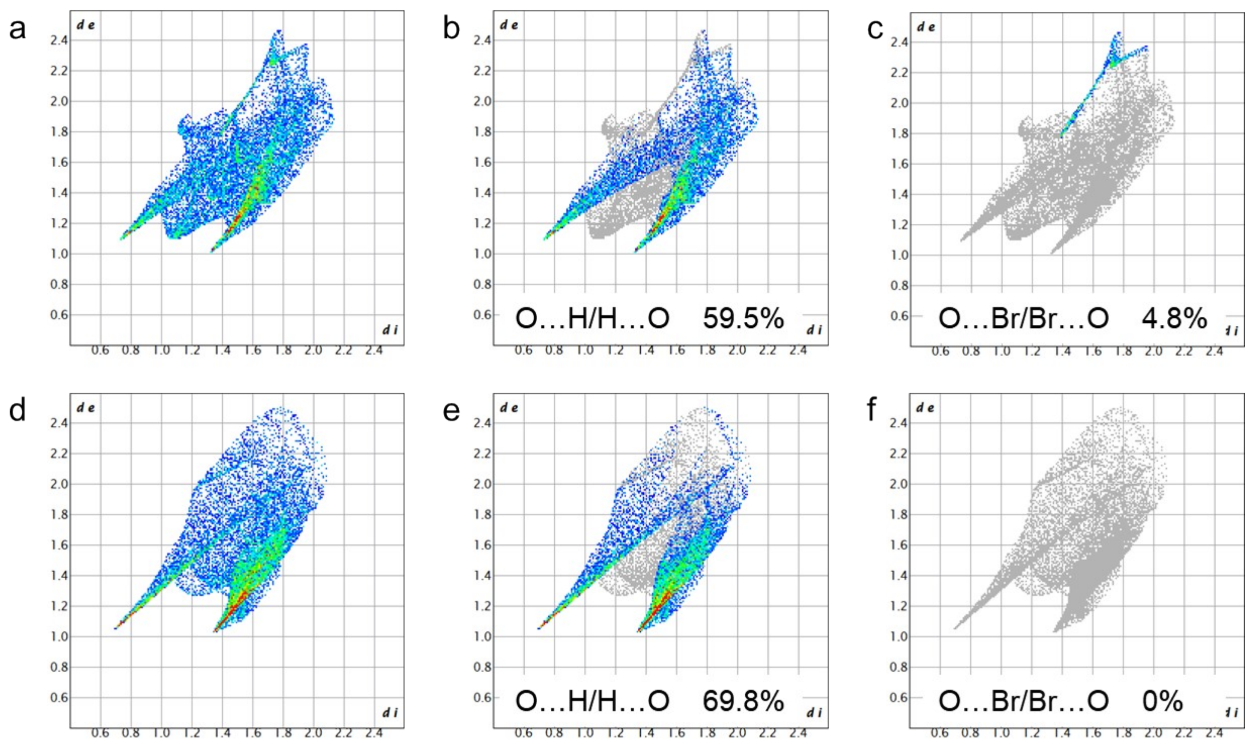

Fig. S12. Fingerprint plots: full (a,d) and resolved into O…H/H…O (b,e) and O…Br/Br…O (c,f) contacts for two crystallographically independent hydrogen peroxide molecules (top and down rows, respectively) in **2**.

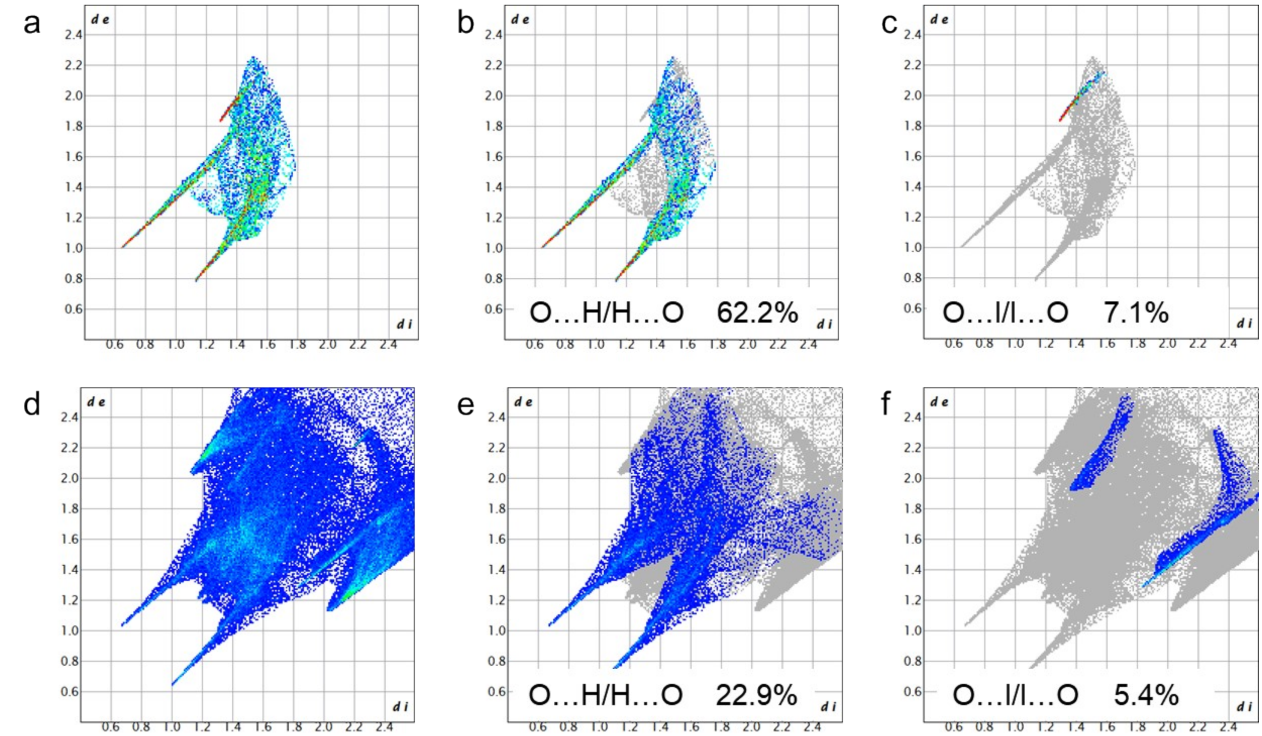

Fig. S13. Fingerprint plots: full (a,d) and resolved into O…H/H…O (b,e) and O…I/I…O (c,f) contacts for hydrogen peroxide (top) and bispidine (down) in **3**.

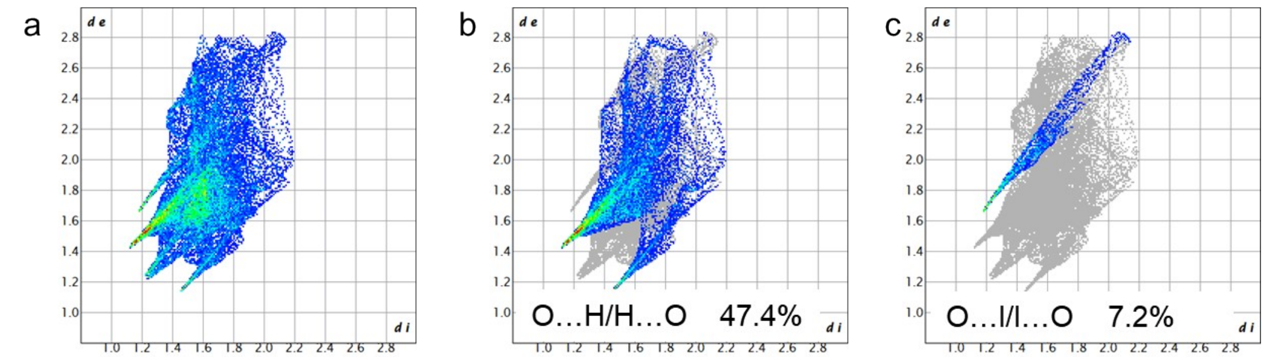

Fig. S14. Fingerprint plots: full (a) and resolved into O…H/H…O (b) and O…I/I…O (c) contacts for diacetone diperoxide molecule in **6**.

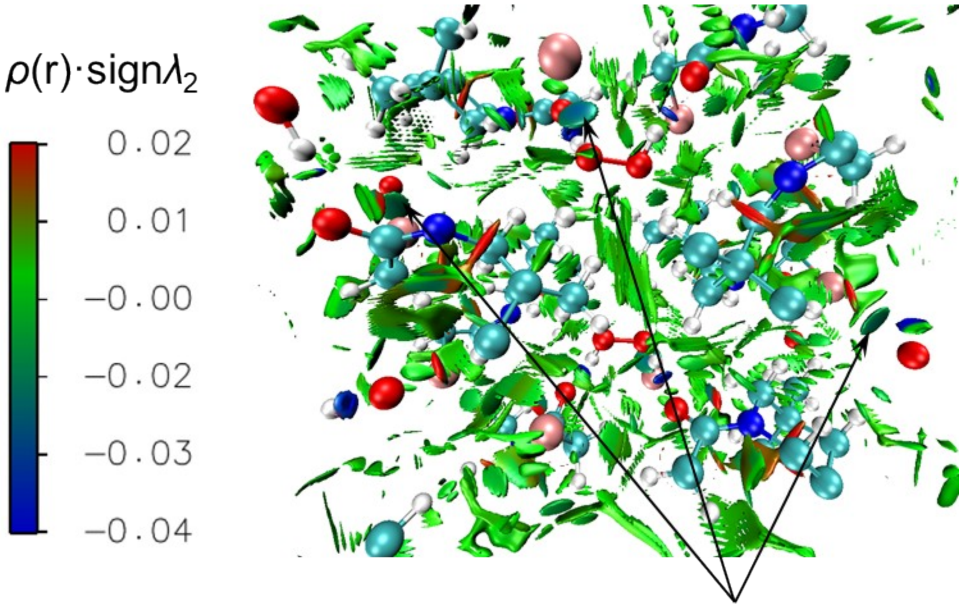

Fig. S15. RDG-based NCI isosurfaces in **1** (RDG isovalue 0.5). The isosurfaces representing halogen bonds are indicated using black arrows. The color scale for ρ(r)□signλ_2 (au) is shown on the left. The I, O, N, C and H atoms are represented by ochre, red, blue, cyan and white spheres, respectively.

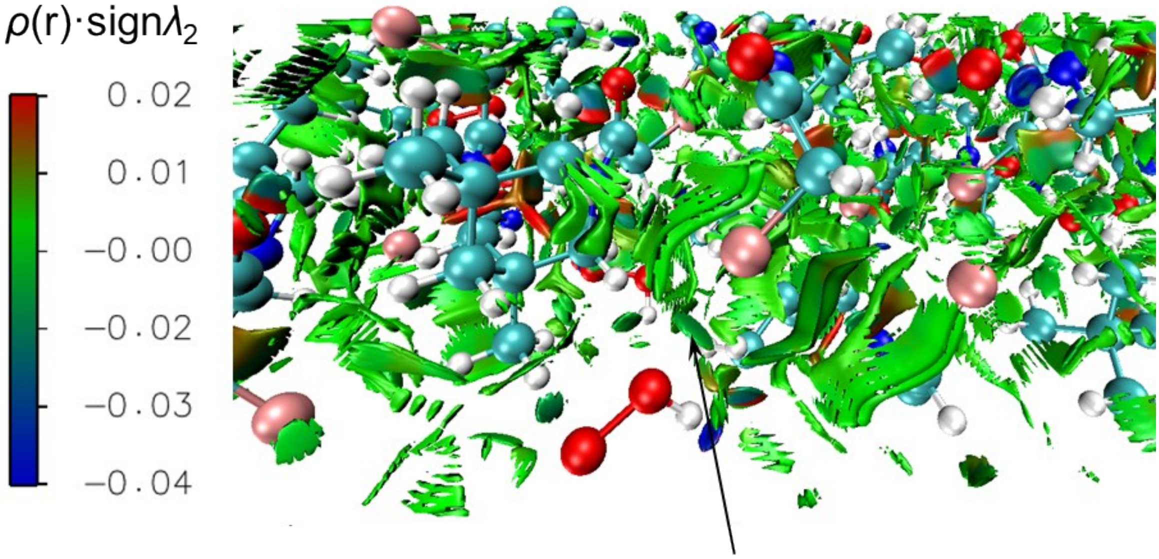

Fig. S16. RDG-based NCI isosurfaces in **2** (RDG isovalue 0.5). The isosurfaces representing halogen bonds are indicated using black arrows. The color scale for ρ(r)□signλ_2 (au) is shown on the left. The Br, O, N, C and H atoms are represented by ochre, red, blue, cyan and white spheres, respectively.

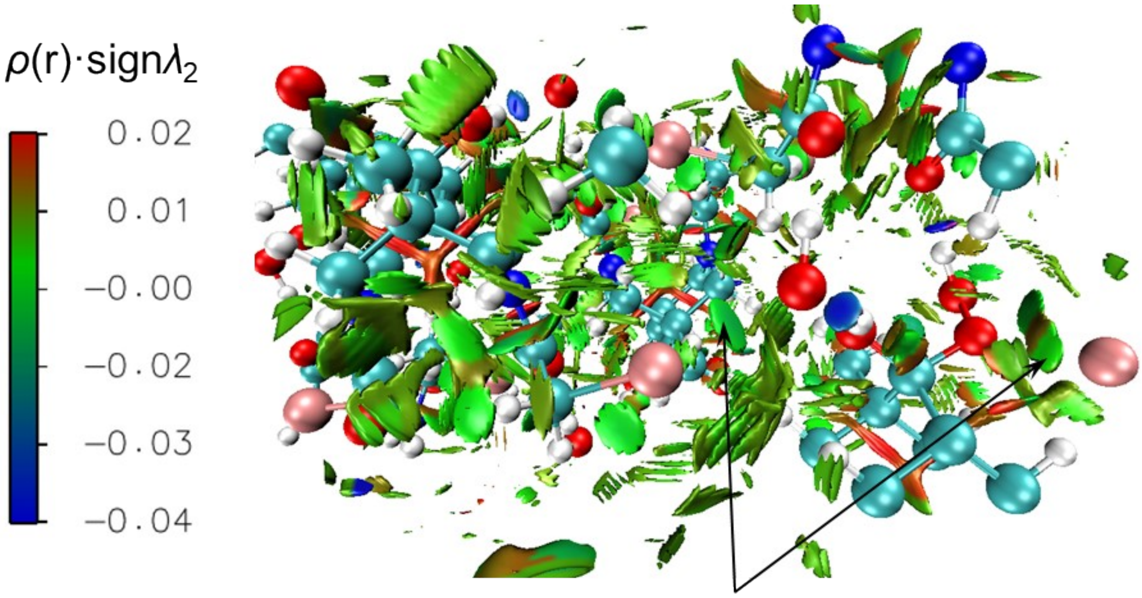

Fig. S17. RDG-based NCI isosurfaces in **3** (RDG isovalue 0.5). The isosurfaces representing halogen bonds are indicated using black arrows. The color scale for ρ(r)signλ_2 (au) is shown on the left. The I, O, N, C and H atoms are represented by ochre, red, blue, cyan and white spheres, respectively.

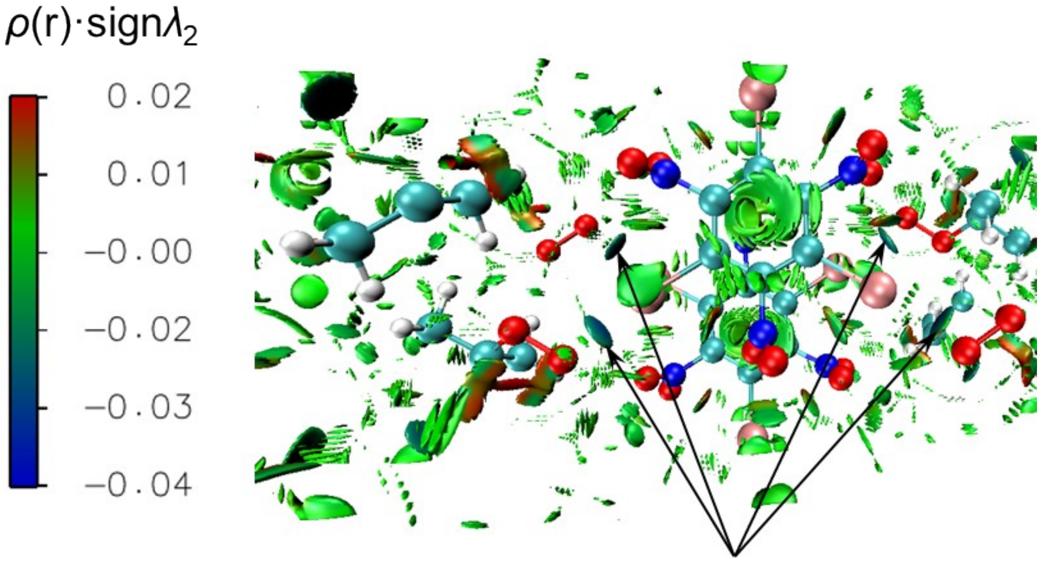

Fig. S18. RDG-based NCI isosurfaces in **6** (RDG isovalue 0.5). The isosurfaces representing halogen bonds are indicated using black arrows. The color scale for ρ(r)signλ_2 (au) is shown on the left. The I, O, N, C and H atoms are represented by ochre, red, blue, cyan and white spheres, respectively.

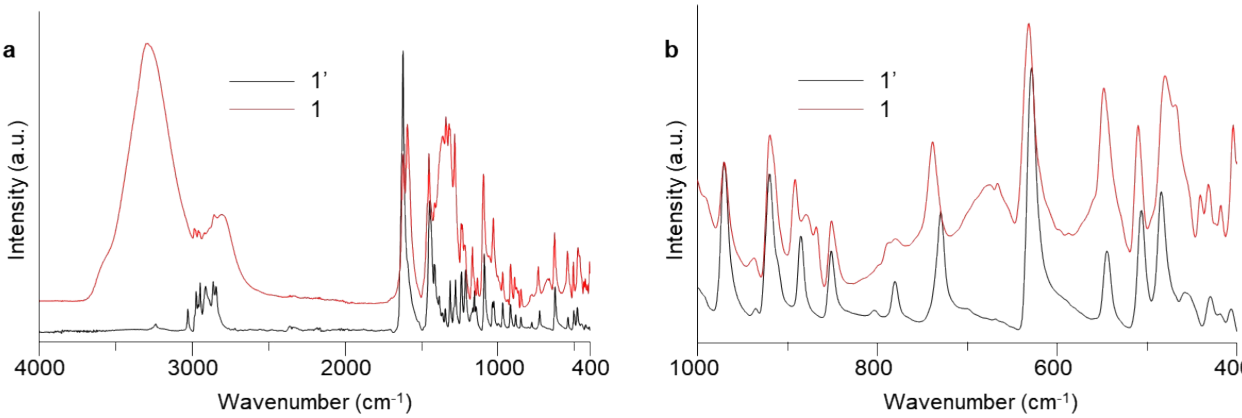

Fig. S19. FTIR spectra of bispidine **1’** and peroxosolvate **1**.

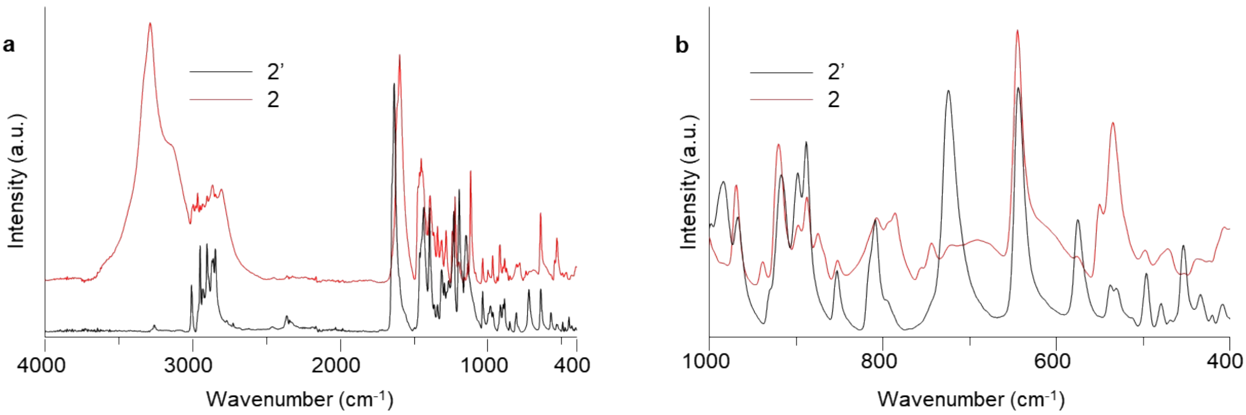

Fig. S20. FTIR spectra of bispidine **2**’ and peroxosolvate **2**.

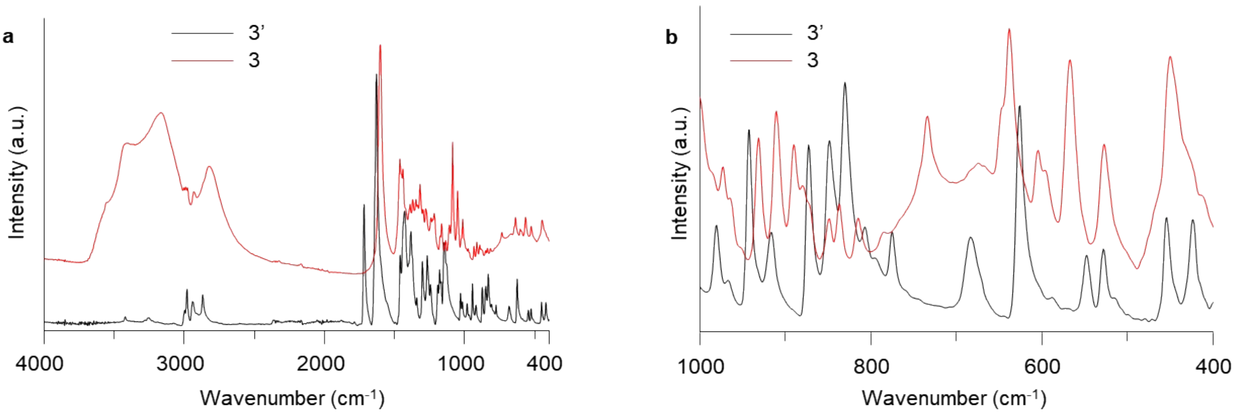

Fig. S21. FTIR spectra of bispidine **3’** and peroxosolvate **3**.

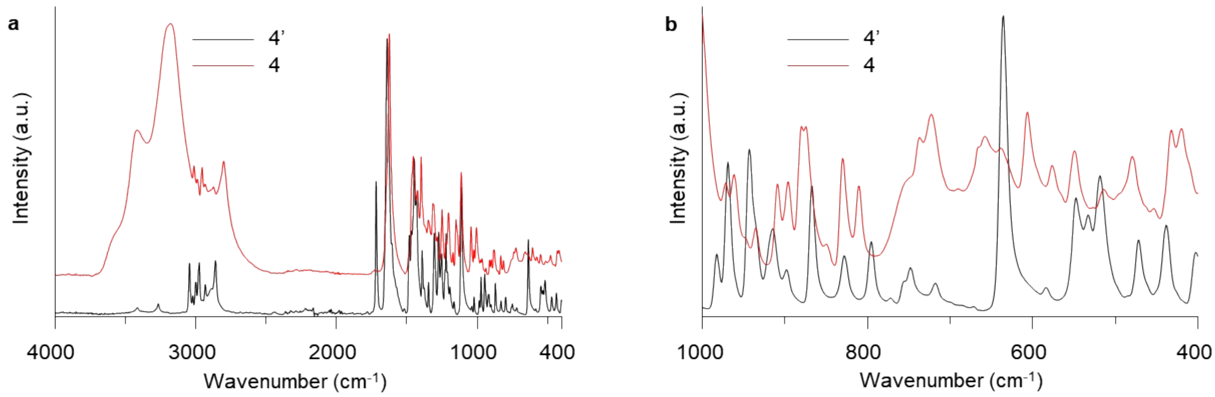

Fig. S22. FTIR spectra of bispidine **4’** and peroxosolvate **4**.

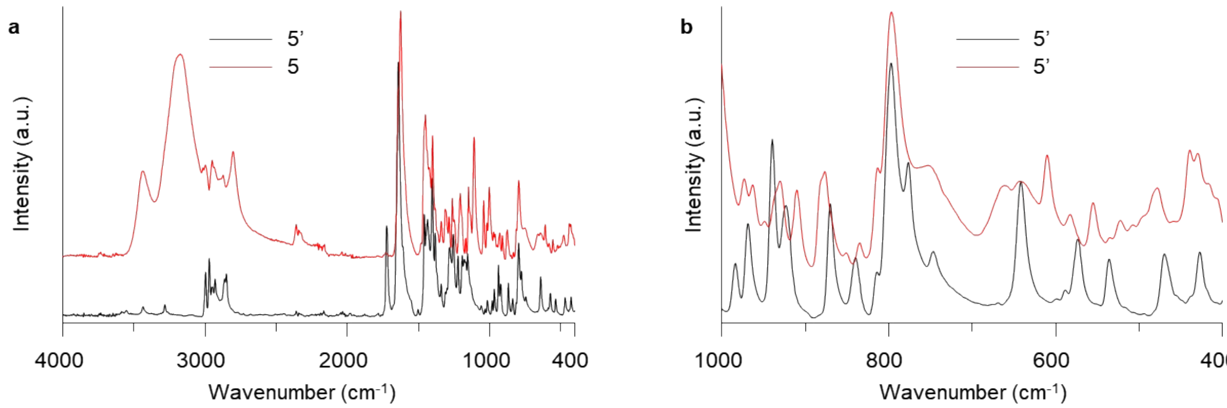

Fig. S23. FTIR spectra of bispidine **5’** and peroxosolvate **5**.

Supplementary Tables.

Table S1. Experimental and optimized parameters of the H-O-O-H…O H-bonds and C-I…O-O intermolecular non-covalent interactions (**1**) at the B3LYP/6-31G** level of theory.

Fragment[a)]	d(O…O), Å		∠(O-H…O), °	
	Exp	Calcd	Exp	Calcd
O(1)-H(1)…O(11)	2.724(4)	2.669	164(5)	169.9
O(2)-H(2)…O(12)[i]	2.777(4)	2.755	171(5)	176.7
O(3)-H(3)…O(21)	2.667(5)	2.683	153(8)	164.8
O(5)-H(5)…O(21)	2.881(9)	- [b)]	157(15)	-
O(4)-H(4)…O(22)[ii]	2.788(7)	2.742	141(10)	168.1
O(6)-H(6)…O(22)[ii]	2.743(8)	-	166(7)	-
	d(I…O), Å		∠(C-I…O), °	
	Exp	Calcd	Exp	Calcd
I(11)…O(2)[iii]	3.152(3)	3.005	162.3(1)	165.7
I(21)…O(3)[iii]	3.034(5)	2.896[b)]	175.6(1)	177.8
I(21)…O(6)[iii]	2.995(9)	-	157.8(2)	-

[a)] See Figs. 1a,b; [b)] Only the major component of disorder was considered for periodic calculations; Symmetry operations i: -X, 1-Y, 2-Z; ii: 1-X, 2-Y, 1-Z; iii: 1+X, Y, Z;

Table S2. Experimental and optimized parameters of the H-O-O-H…O H-bonds and C-Br…O-O intermolecular non-covalent interactions (**2**) at the B3LYP/6-31G** level of theory.

Fragment[a)]	d(O…O), Å		∠(O-H…O), °	
	Exp	Calcd	Exp	Calcd
O(5)-H(5)…O(4)[ii]	2.748(5)	2.725	163(6)	167.0
O(6)-H(6)…O(3)	2.708(4)	2.680	165(6)	176.3
O(7)-H(7)…O(2)[iii]	2.738(5)	2.718	167(7)	171.2
O(8)-H(8)…O(1)	2.719(6)	2.667	156(7)	170.6
O(9)-H(9)…O(2)	2.87(2)	-[b)]	179.8	-
O(10)-H(10)…O(1)	2.58(2)	-	179(9)	-
	d(Br…O), Å		∠(C-Br…O), °	
	Exp	Calcd	Exp	Calcd
Br(1)…O(8)[i]	3.172(5)	3.029	161.8(2)	167.4

[a)] See Fig. 2; i: X, -1+Y, +Z; ii: -X+1, Y-1/2, -Z+ 3/2; iii: -X+2, -Y, -Z+1; [b)] Only the major component of disorder was considered for periodic calculations.

Table S3. Experimental and optimized parameters of the H-O-O-H…O H-bonds and C-I…O-O intermolecular non-covalent interactions (**3)** at the B3LYP/6-31G** level of theory.

Fragment[a)]	d(O…O), Å		∠(O-H…O), °	
	Exp	Calcd	Exp	Calcd
O(7)-H(7)…O(1)	2.620(8)	2.549	171.7	176.1
O(4)-H(4)…O(2)[v b)]	2.74(2)	-	157.3	-
O(6)-H(6)…O(2)[v]	2.695(9)	2.672	176.4	168.8
O(3)-H(3)…O(7)[v]	2.798(8)	2.744	150.1	147.8
	d(I…O), Å		∠(C-I…O), °	
	Exp	Calcd	Exp	Calcd
I(1)…O(7)[ii]	3.127(5)	3.125	166.1(2)	162.8
I(2)…O(6)[i]	3.296(7)	3.159[b)]	164.9(2)	167.7

[a)] See Fig. 3; i: -X+2, -Y+1, -Z+1; ii: -X+1, Y+1/2, -Z+3/2; v: X, Y+1, Z; [b)] Only the major component of disorder was considered for periodic calculations.

Table S4. Geometric parameters of the O-H…O H-bonds in **4** and **5**.

Fragment[a)]	d(H…O), Å	d(O…O), Å	∠(O-H…O), °	d(H…O), Å	d(O…O), Å	∠(O-H…O), °
	4			**5**		
O(2)-H(2)…O(4)	2.22(7)	3.002(5)	152(14)	2.22(4)	3.015(2)	152(4)
O(3)-H(3)…O(4)	1.80(4)	2.610(7)	160(11)	1.73(5)	2.597(3)	164(5)
O(4)[ii]-H(4)[ii]…O(1)	1.85(2)	2.672(4)	162(6)	1.88(2)	2.656(2)	155(3)

[a)] See Fig. S1; ii: X-1/2, Y+1/2, Z.

Table S5. Computed values of the electron density, ρ_b, the local electronic kinetic energy density, G_b, potential energy density, V_b at the O…O interaction critical point and the H-bond energy values E_{HB} evaluated using Eqs. S1, S2 in **1**.

H-bonded/O2XB fragment[a)]	ρ_b (a.u.)	V_b (a.u.)	G_b (a.u.)	E_{int}[b)]	E_{int}[c)]
				(kJ mol^{-1})	
O(1)-H(1)…O(11)	0.0439	-0.0341	0.0344	**44.7**	**38.7**
O(2)-H(2)…O(12)[i]	0.0372	-0.0270	0.0274	**35.4**	**30.8**
O(3)-H(3)…O(21)	0.0390	-0.0298	0.0315	**39.1**	**35.4**
O(4)-H(4)…O(22)[ii]	0.0386	-0.0284	0.0281	**37.2**	**31.6**

[a)] See Fig. 1; [b)] see Eq. S1; [c)] see Eq. S2; Symmetry operations i: -X, 1-Y, 2-Z; ii: 1-X, 2-Y, 1-Z; iii: 1+X, Y, Z;

Table S6. Computed values of the electron density, ρ_b, the local electronic kinetic energy density, G_b, potential energy density, V_b at the O…O interaction critical point and the H-bond energy values E_{HB} evaluated using Eqs. S1, S2 in **2**.

H-bonded/O2XB fragment[a)]	ρ_b (a.u.)	V_b (a.u.)	G_b (a.u.)	E_{int}[b)]	E_{int}[c)]
				(kJ mol^{-1})	
O(5)-H(5)…O(4)^{ii}	0.0366	-0.0274	0.0286	**35.9**	**32.2**
O(6)-H(6)…O(3)	0.0458	-0.0349	0.0344	**45.8**	**38.7**
O(7)-H(7)…O(2)^{iii}	0.0408	-0.0306	0.0304	**40.1**	**34.2**
O(8)-H(8)…O(1)	0.0439	-0.0341	0.0348	**44.7**	**39.1**

[a)] See Fig. 2; [b)] see Eq. S1; [c)] see Eq. S2; Symmetry operations i: X, -1+Y, +Z; ii: -X+1, Y-1/2, -Z+ 3/2; iii: -X+2, -Y, -Z+1.

Table S7. Computed values of the electron density, ρ_b, the local electronic kinetic energy density, G_b, potential energy density, V_b at the O…O interaction critical point and the H-bond/O2XB energy values E_{HB} evaluated using Eqs. S1, S2 in **3**.

H-bonded/O2XB fragment[a)]	ρ_b (a.u.)	V_b (a.u.)	G_b (a.u.)	E_{int}[b)]	E_{int}[c)]
				(kJ mol^{-1})	
O(7)-H(7)…O(1)	0.0671	-0.061	0.0519	**80.0**	**58.4**
O(6)-H(6)…O(2)^{v}	0.0463	-0.035	0.0342	**45.9**	**38.5**
O(3)-H(3)…O(7)^{v}	0.0315	-0.024	0.0232	**31.5**	**26.1**

[a)] See Fig. 3; [b)] see Eq. S1; [c)] see Eq. S2; Symmetry operations i: -X+2, -Y+1, -Z+1; ii: -X+1, Y+1/2, -Z+3/2; v: X, Y+1, Z

Table S8. Computed values of the electron density, ρ_b, the local electronic kinetic energy density, G_b, potential energy density, V_b at the Hal…O interaction critical point and the Hal…O energy values E_{int} evaluated using Eqs. S1-S4.

Compound	Fragment	ρ_b	V_b	G_b	E_{int}[a)]	E_{int}[b)]	E_{int}[c)]
		a.u.			kJ mol^{-1}		
1[d)]	I(11)…O(2)	0.0162	-0.0110	0.0113	14.4	19.6	19.9
	I(21)…O(3)	0.0204	-0.0142	0.0142	18.6	25.3	25.0
2[e)]	Br(1)…O(8)	0.0103	-0.0068	0.0081	8.9	10.3	12.1
3[f)]	I(1)…O(7)	0.0130	-0.0087	0.0090	11.4	15.5	15.8
	I(2)…O(6)	0.0117	-0.0079	0.0084	10.4	14.1	14.8
6	I…O	0.0225	-0.0164	0.0171	21.5	28.8	30.0

[a)] see Eq. S1; [b)] see Eq. S3; [c)] see Eq. S4;[d)] See Fig. 1b; [e)] See Fig. 2; [f)] See Fig. 3.

Table S9. X-ray structure determination summary.

Compound	**2**	**3**	**4**	**5**
Empirical formula	$C_{13}H_{20}Br_2N_2O_2 \cdot H_2O_2$	$C_{13}H_{20}I_2N_2O_5 \cdot 0.5H_2O_2$	$C_{13}H_{20}Br_2N_2O_5 \cdot H_2O_2$	$C_{13}H_{20}Cl_2N_2O_5 \cdot H_2O_2$
F_w	430.14	555.12	478.14	389.26
Crystal system	Monoclinic	Monoclinic	Monoclinic	Monoclinic
Space group	$P2_1/c$	$P2_1/c$	$C2/c$	$C2/c$
a/Å	15.8307(10)	13.6546(5)	7.1669(7)	7.1348(3)
b/Å	7.7891(5)	8.6106(3)	20.9465(16)	20.9560(8)
c/Å	26.3237(17)	15.3908(7)	11.2346(10)	11.0766(4)
$\alpha/^o$	90	90	90	90
$\beta/^o$	90.248(2)	104.962(2)	93.934(4)	94.251(1)
$\gamma/^o$	90	90	90	90
V/Å^3	3245.9(4)	1748.21(12)	1682.6(3)	1651.58(11)
Z	8	4	4	4
F(000)	1728	1068	960	816
d_{calc}/g•cm^{-3}	1.760	2.109	1.888	1.566
μ/mm^{-1}	5.01	3.628	4.857	0.433
T/K	100	100	100	100
Data collected	35478	12198	6415	13470
Unique data (R_{int})	5811 (0.058)	3075 (0.047)	1657 (0.064)	2199 (0.0293)
Reflections with $I>2\sigma(I)$	4704	2609	1366	1940
θ range/°	2.01-25.15	1.54-25.00	1.94-25.99	1.94-28.99
No of variables	405	220	123	128
R_1 [$I>2\sigma(I)$]	0.041	0.050	0.039	0.037
wR_2 (all data)	0.094	0.092	0.092	0.092
GOF	1.033	1.196	1.158	1.074
$\Delta\rho_{max,min}$/e Å^{-3}	2.55 / -1.82	1.27 / -1.28	0.49 / -0.49	0.35 / -0.19
CCDC	2289223	2289224	2289225	2289226

References:

1 Y. Wolanov, O. Lev, A. V. Churakov, A. G. Medvedev, V. M. Novotortsev and P. V. Prikhodchenko, Preparation of pure hydrogen peroxide and anhydrous peroxide solutions from crystalline serine perhydrate, *Tetrahedron*, 2010, **66**, 5130–5133.

2 W. C. Schumb, C. N. Satterfield and R. L. Wentworth, *Hydrogen peroxide*, Reinhold Publishing Corporation, New York, 1955.

3 A. V. Churakov, A. V. Medved'ko, P. V. Prikhodchenko, D. P. Krut'ko and S. Z. Vatsadze, First example of peroxosolvate of iodine-containing organic molecule, *Mendeleev Commun.*, 2021, **31**, 352–355.

4 A. V. Medved'ko, B. V. Egorova, A. A. Komarova, R. D. Rakhimov, D. P. Krut'ko, S. N. Kalmykov and S. Z. Vatsadze, Copper–Bispidine Complexes: Synthesis and Complex Stability Study, *ACS Omega*, 2016, **1**, 854–867.

5 D. P. Krut'ko, A. V. Medved'ko, K. A. Lyssenko, A. V. Churakov, A. I. Dalinger, M. A. Kalinin, A. O. Gudovannyy, K. Y. Ponomarev, E. V. Suslov and S. Z. Vatsadze, Bispidine Platform as a Tool for Studying Amide Configuration Stability, *Molecules*, 2022, **27**, 430.

6 G. M. Sheldrick, SADABS, Programs for Scaling and Absorption Correction of Area Detector Data, *SADABS ver. 2016/2 - Bruker AXS area Detect. scaling Absorpt. Correct. Progr.*, 2016, Bruker AXS, Karlsruhe, Germany.

7 G. M. Sheldrick, Crystal structure refinement with SHELXL, *Acta Crystallogr. Sect. C Struct. Chem.*, 2015, **71**, 3–8.

8 M. A. Spackman and D. Jayatilaka, Hirshfeld surface analysis, *CrystEngComm*, 2009, **11**, 19–32.

9 P. R. Spackman, M. J. Turner, J. J. McKinnon, S. K. Wolff, D. J. Grimwood, D. Jayatilaka and M. A. Spackman, CrystalExplorer : a program for Hirshfeld surface analysis, visualization and quantitative analysis of molecular crystals, *J. Appl. Crystallogr.*, 2021, **54**, 1006–1011.

10 R. Dovesi, A. Erba, R. Orlando, C. M. Zicovich-Wilson, B. Civalleri, L. Maschio, M. Rérat, S. Casassa, J. Baima, S. Salustro and B. Kirtman, Quantum-mechanical condensed matter simulations with CRYSTAL, *WIREs Comput. Mol. Sci.*, , DOI:10.1002/wcms.1360.

11 J. Laun, D. Vilela Oliveira and T. Bredow, Consistent gaussian basis sets of double- and triple-zeta valence with polarization quality of the fifth period for solid-state calculations, *J. Comput. Chem.*, 2018, **39**, 1285–1290.

12 J. P. Perdew, K. Burke and M. Ernzerhof, Generalized Gradient Approximation Made Simple, *Phys. Rev. Lett.*, 1996, **77**, 3865–3868.

13 S. Grimme, S. Ehrlich and L. Goerigk, Effect of the damping function in dispersion corrected density functional theory, *J. Comput. Chem.*, 2011, **32**, 1456–1465.

14 C. Gatti and S. Cassasa, *TOPOND14 User's Manual*, CNR-ISTM of Milano, Milano, Italy, 2013.

15 G. Saleh, L. Lo Presti, C. Gatti and D. Ceresoli, NCImilano : an electron-density-based code for the study of noncovalent interactions, *J. Appl. Crystallogr.*, 2013, **46**, 1513–1517.

16 W. Humphrey, A. Dalke and K. Schulten, VMD: Visual molecular dynamics, *J. Mol. Graph.*, 1996, **14**, 33–38.

17 V. G. Tsirelson, in *The Quantum Theory of Atoms in Molecules*, Wiley-VCH Verlag GmbH & Co. KGaA, Weinheim, Germany, 2007, pp. 257–283.

18 R. F. W. Bader, A quantum theory of molecular structure and its applications, *Chem. Rev.*, 1991, **91**, 893–928.

19 A. V. Churakov, D. A. Grishanov, A. G. Medvedev, A. A. Mikhaylov, T. A. Tripol'skaya,

M. V. Vener, M. A. Navasardyan, O. Lev and P. V. Prikhodchenko, Cyclic dipeptide peroxosolvates: first direct evidence for hydrogen bonding between hydrogen peroxide and a peptide backbone, *CrystEngComm*, 2019, **21**, 4961–4968.
20 A. G. Medvedev, A. A. Mikhaylov, I. Y. Chernyshov, M. V. Vener, O. Lev and P. V. Prikhodchenko, Effect of aluminum vacancies on the H 2 O 2 or H 2 O interaction with a gamma-AlOOH surface. A solid-state DFT study, *Int. J. Quantum Chem.*, 2019, **119**, e25920.
21 E. Espinosa, E. Molins and C. Lecomte, Hydrogen bond strengths revealed by topological analyses of experimentally observed electron densities, *Chem. Phys. Lett.*, 1998, **285**, 170–173.
22 I. Mata, I. Alkorta, E. Espinosa and E. Molins, Relationships between interaction energy, intermolecular distance and electron density properties in hydrogen bonded complexes under external electric fields, *Chem. Phys. Lett.*, 2011, **507**, 185–189.
23 M. V. Vener, A. N. Egorova, A. V. Churakov and V. G. Tsirelson, Intermolecular hydrogen bond energies in crystals evaluated using electron density properties: DFT computations with periodic boundary conditions, *J. Comput. Chem.*, 2012, **33**, 2303–2309.
24 E. V Bartashevich and V. G. Tsirelson, Interplay between non-covalent interactions in complexes and crystals with halogen bonds, *Russ. Chem. Rev.*, 2014, **83**, 1181–1203.
25 M. H. Kolář and P. Hobza, Computer Modeling of Halogen Bonds and Other σ-Hole Interactions, *Chem. Rev.*, 2016, **116**, 5155–5187.
26 M. J. Frisch, G. W. Trucks, H. B. Schlegel, G. E. Scuseria, M. A. Robb, J. R. Cheeseman, G. Scalmani, V. Barone, B. Mennucci, G. A. Petersson, H. Nakatsuji, M. Caricato, X. Li, H. P. Hratchian, A. F. Izmaylov, J. Bloino, G. Zheng, J. L. Sonnenberg, M. Hada, M. Ehara, K. Toyota, R. Fukuda, J. Hasegawa, M. Ishida, T. Nakajima, Y. Honda, O. Kitao, H. Nakai, T. Vreven, J. A. Montgomery Jr., J. E. Peralta, F. Ogliaro, M. Bearpark, J. J. Heyd, E. Brothers, K. N. Kudin, V. N. Staroverov, R. Kobayashi, J. Normand, K. Raghavachari, A. Rendell, J. C. Burant, S. S. Iyengar, J. Tomasi, M. Cossi, N. Rega, J. M. Millam, M. Klene, J. E. Knox, J. B. Cross, V. Bakken, C. Adamo, J. Jaramillo, R. Gomperts, R. E. Stratmann, O. Yazyev, A. J. Austin, R. Cammi, C. Pomelli, J. W. Ochterski, R. L. Martin, K. Morokuma, V. G. Zakrzewski, G. A. Voth, P. Salvador, J. J. Dannenberg, S. Dapprich, A. D. Daniels, Ö. Farkas, J. B. Foresman, J. V Ortiz, J. Cioslowski and D. J. Fox, *Gaussian Inc., Wallingford CT*, 2009, Wallingford CT.